

Article

Not peer-reviewed version

Mechanisms of Low-Temperature Dislocation Motion in High-Entropy $\text{Al}_{0.5}\text{CoCrCuFeNi}$ Alloy

[Yuri Semerenko](#) ^{*}, Vasilij Natsik, Elena Tabachnikova, [Yi Huang](#), [Terence G. Langdon](#)

Posted Date: 7 June 2024

doi: [10.20944/preprints202406.0418.v1](https://doi.org/10.20944/preprints202406.0418.v1)

Keywords: high-entropy alloy; cryogenic temperatures; acoustic relaxation; plastic deformation; low-temperature plasticity



Preprints.org is a free multidiscipline platform providing preprint service that is dedicated to making early versions of research outputs permanently available and citable. Preprints posted at Preprints.org appear in Web of Science, Crossref, Google Scholar, Scilit, Europe PMC.

Copyright: This is an open access article distributed under the Creative Commons Attribution License which permits unrestricted use, distribution, and reproduction in any medium, provided the original work is properly cited.

Disclaimer/Publisher's Note: The statements, opinions, and data contained in all publications are solely those of the individual author(s) and contributor(s) and not of MDPI and/or the editor(s). MDPI and/or the editor(s) disclaim responsibility for any injury to people or property resulting from any ideas, methods, instructions, or products referred to in the content.

Article

Mechanisms of Low-Temperature Dislocation Motion in High-Entropy Al_{0.5}CoCrCuFeNi Alloy

Yu.O. Semerenko ^{1,*}, V.D. Natsik ¹, E.D. Tabachnikova ¹, Yi Huang ² and T.G. Langdon ³

¹ B.Verkin Institute for Low Temperature Physics and Engineering of the National Academy of Sciences of Ukraine, 47 Nauky Ave., Kharkiv, 61103, Ukraine

² Department of Design and Engineering, Faculty of Science and Technology, Bournemouth University, Poole, Dorset BH12 5BB, UK

³ Department of Mechanical Engineering, University of Southampton, Southampton SO17 1BJ, UK

* Correspondence: semerenko@ilt.kharkov.ua

Abstract: An analysis of the processes of plastic deformation and acoustic relaxation in a high-entropy alloy Al_{0.5}CoCrCuFeNi was carried out. The following have been established: dominant dislocation defects; types of barriers that prevent the movement of dislocations; mechanisms of thermally activated movement of various elements of dislocation lines through barriers at room and low temperatures. Based on modern dislocation theory, quantitative estimates have been obtained for the most important characteristics of dislocations and their interaction with barriers.

Keywords: high-entropy alloy; cryogenic temperatures; acoustic relaxation; plastic deformation; low-temperature plasticity

1. Introduction

At the beginning of the 21st century, two articles [1] appeared, in which a new strategy for the development of new multicomponent metal alloys was proposed. These alloys are called high-entropy alloys (HEA), since they have an increased entropy of mixing. Their structure consists of different major elements in the range of 5–35 atomic percent and typically contains a single phase, instead of the many metallic phases formed in the structure of traditional alloys. Due to their structural features, HEA have many improved mechanical properties: increased strength and ductility, high fracture toughness at both high and low temperatures, good wear resistance, increased resistance to corrosion and oxidation [3–8]. In this regard, many articles have appeared in the literature studying the mechanical properties of HEA using active deformation methods in a wide range of both high and low temperatures [9–20]. At the same time, the number of studies of HEA at small deformations in the elastic region is clearly not enough. Obviously, this restrained the establishment of the physical mechanisms responsible for the plastic deformation of HEA. It is known that one of the main methods for studying deformations in the elastic region is the method of resonance spectroscopy. It makes it possible to excite cyclic elastic deformation in samples with an amplitude of $\sim 10^{-7}$, caused by short segments of dislocation strings (dislocation relaxers), which oscillate with amplitudes on the order of the lattice parameter. Previously, we used this method at temperatures $T < 300$ K to measure the acoustic properties (features temperature dependences of internal friction, dynamic Young's modulus) and mechanical properties (under uniaxial compression and tension) in one of the typical Al_{0.5}CoCrCuFeNi HEAs with an fcc lattice [21,22].

In this publication, we will take a closer look at the relationship between this properties and the features of the dynamics and kinetics of elementary dislocation processes in this alloy. We will also discuss the possibility of using the fundamental principles of modern dislocation theory to interpret these properties. We use data from two different experimental methods with different intensities of influence on the dislocation structure in the studied alloy samples:

- method of resonant mechanical spectroscopy – excitation in samples of cyclic elastic deformation with an amplitude of $\varepsilon_0 \sim 10^{-7}$, caused by short segments of dislocation strings (dislocation relaxers), which oscillate with amplitudes on the order of the lattice parameter;
- method of active deformation, when used, significant plastic deformations of $\varepsilon \sim 3 \cdot 10^{-1}$ are achieved, caused by the translational movement of extended dislocations over macroscopic distances.

2. Materials and Methods of Research

The production method and characteristics of the alloy are described in [21,22]. The alloy was studied in 2 structural states: (I) - initial cast; (II) - after high-temperature annealing in vacuum at 975 °C for 6 hours. It has been shown [23] that the distribution of elements included in the alloy is non-uniform at the nanoscale. In the microstructure of the alloy, regions are observed in the form of stripes 15-20 nm wide, with significantly different concentrations of various elements; such regions form a three-dimensional irregular lattice in the microstructure. Significant structural distortions are observed near the lattice nodes. The distance between these inhomogeneities is equal to ~ 20 nm. In addition, clusters of several atoms of one of the constituent elements of the alloy are observed. Several adjacent atoms of an element with a relatively large atomic radius create local distortions of the crystal lattice. The characteristic distance between clusters is several nanometers.

3. Experimental Results

3.1. Acoustic Properties

The temperature dependences of internal friction $Q_{\text{exp}}^{-1}(T)$ and dynamic Young's modulus $E_{\text{exp}}(T)$ were studied in [22] using the method of mechanical resonance spectroscopy. The technique for measuring acoustic absorption (internal friction) and dynamic Young's modulus in these experiments is described in [24].

As the temperature decreases, $E_{\text{exp}}(T)$ for state (I) increases monotonically and $Q_{\text{exp}}^{-1}(T)$ decreases monotonically, while the temperature dependences $Q_{\text{exp}}^{-1}(T)$ and $E_{\text{exp}}(T)$ do not show any significant features such as relaxation resonances.

The transition to state (II) leads to the appearance of a relaxation resonance - an acoustic absorption peak and a corresponding step in the temperature dependence of the dynamic modulus (Figure 1).

To interpret the acoustic relaxation resonances observed in experiments [22], it is necessary to carry out initial processing of the measurement results of $E_{\text{exp}}(T)$ and $Q_{\text{exp}}^{-1}(T)$: to identify on these temperature dependences the resonant contributions $E_R(T)$ and $Q_R^{-1}(T)$ individual subsystems of relaxers against the background of contributions $E_{BG}(T)$ and $Q_{BG}^{-1}(T)$ other relaxation processes.

In general, the dynamic modulus of elasticity depends on both temperature T and frequency ω . However, our measurements were performed at a fixed value of the sample oscillation frequency $\omega_r = 2\pi f_r$. It has been established [24] that the dependence $E_{\text{exp}}(T, \omega)$ recorded in experiments can be divided into resonant $E_R(T, \omega)$ and background $E_{BG}(T, \omega)$ components:

$$E_{\text{exp}}(T, \omega) = E_0(\omega) - E_{BG}(T, \omega) - E_R(T, \omega) \quad (1)$$

where $E_0(\omega)$ is the limit value of the module at $T \rightarrow 0$. For most crystalline materials, the value E_0 is close to the value of the static modulus of elasticity of a dislocation-free crystal.

According to [25], for many crystalline materials the background component $E_{BG}(T, \omega)$ in the region of low temperatures $T < 300$ K and frequencies $\omega \leq 10^7$ s⁻¹ is determined primarily by the interaction of elastic vibrations with thermal phonons. For the Einstein model of the phonon spectrum with a characteristic temperature Θ_E , the softening of the elastic modulus by phonons is described by the formula

$$\frac{E_{BG}(T, \omega)}{E_0(\omega)} = \beta \cdot T \exp\left(-\frac{T_\eta}{T}\right), \quad (2)$$

where the coefficient β depends on the material under study and the vibration mode under study, and the characteristic temperature T_η in most cases for materials with simple phonon spectra is of the order of the Einstein Θ_E or Debye Θ_D temperatures: $T_\eta \leq \Theta_E = h\nu_E \approx \frac{3}{4}\Theta_D$ (h - Planck constant), since in real crystals the frequencies of acoustic phonons are lower than the Einstein frequency ν_E [26]. In the simplest case $\Theta_E = \frac{3}{4}\Theta_D$.

In the temperature range $T \leq 10$ K, along with the phonon contribution (2), one can also distinguish a relatively weak electronic contribution in $E_{BG}(T, \omega)$ [24], but it does not play a significant role in the analysis of dynamic elastic moduli in the temperature range $T < \Theta_D$.

$$\text{Then: } E_{\text{exp}}(T, \omega) = E_0(\omega) \cdot \eta(T) - E_R(T, \omega), \quad \eta(T) = 1 - \beta T \exp(-T_\eta/T) \quad (3)$$

It has been shown [21], that (3) well describes the $E_{\text{exp}}(T, \omega)$ of alloy under study in the absence of relaxation resonances, when $E_R(T, \omega) \equiv 0$ (state **I**). Its use for approximating the results obtained when studying state **(II)** is illustrated in Figure 1a (solid line), and the corresponding parameter values are given in Table 1. When transitioning from state **(I)** to state **(II)**, the parameter E_0 increases, but the characteristic temperature T_η and coefficient β remain unchanged.

The temperature dependence of the resonant component of the Young's modulus for state **(II)** is shown in Figure 1a. Its graph has the shape of a step with a height characteristic of relaxation resonances $E_{R0} = E_R(T \gg T_p, \omega)$ (Table 1).

$$E_R(T, \omega) = E_0(\omega) \cdot \eta(T) - E_{\text{exp}}(T, \omega) \quad (4)$$

Table 1. Parameters of background $E_{BG}(T, \omega)$ and $Q_{BG}^{-1}(T)$ for HEA Al_{0.5}CoCrCuFeNi in state **(II)**.

| $\omega = 2\pi f_r$ | E_0 | β | T_η | E_{R0} | A_1 | A_2 | U_{BG} |
|-----------------------------------|---------|-------------------------------------|----------|----------|-------------------|-------|----------|
| $3.34 \cdot 10^3$ s ⁻¹ | 236 GPa | $3.5 \cdot 10^{-4}$ K ⁻¹ | 160 K | 0.33 GPa | $6 \cdot 10^{-5}$ | 0.3 | 0.16 eV |

The experimentally observed dependence $Q_{\text{exp}}^{-1}(T, \omega)$ consists of the sum of resonant $Q_R^{-1}(T, \omega)$ and background $Q_{BG}^{-1}(T, \omega)$ absorption. The interpretation of the internal friction

peaks recorded in the experiment comes down to a comparison with the theory of the difference value

$$Q_R^{-1}(T, \omega) = Q_{\text{exp}}^{-1}(T, \omega) - Q_{\text{BG}}^{-1}(T, \omega) \quad (5)$$

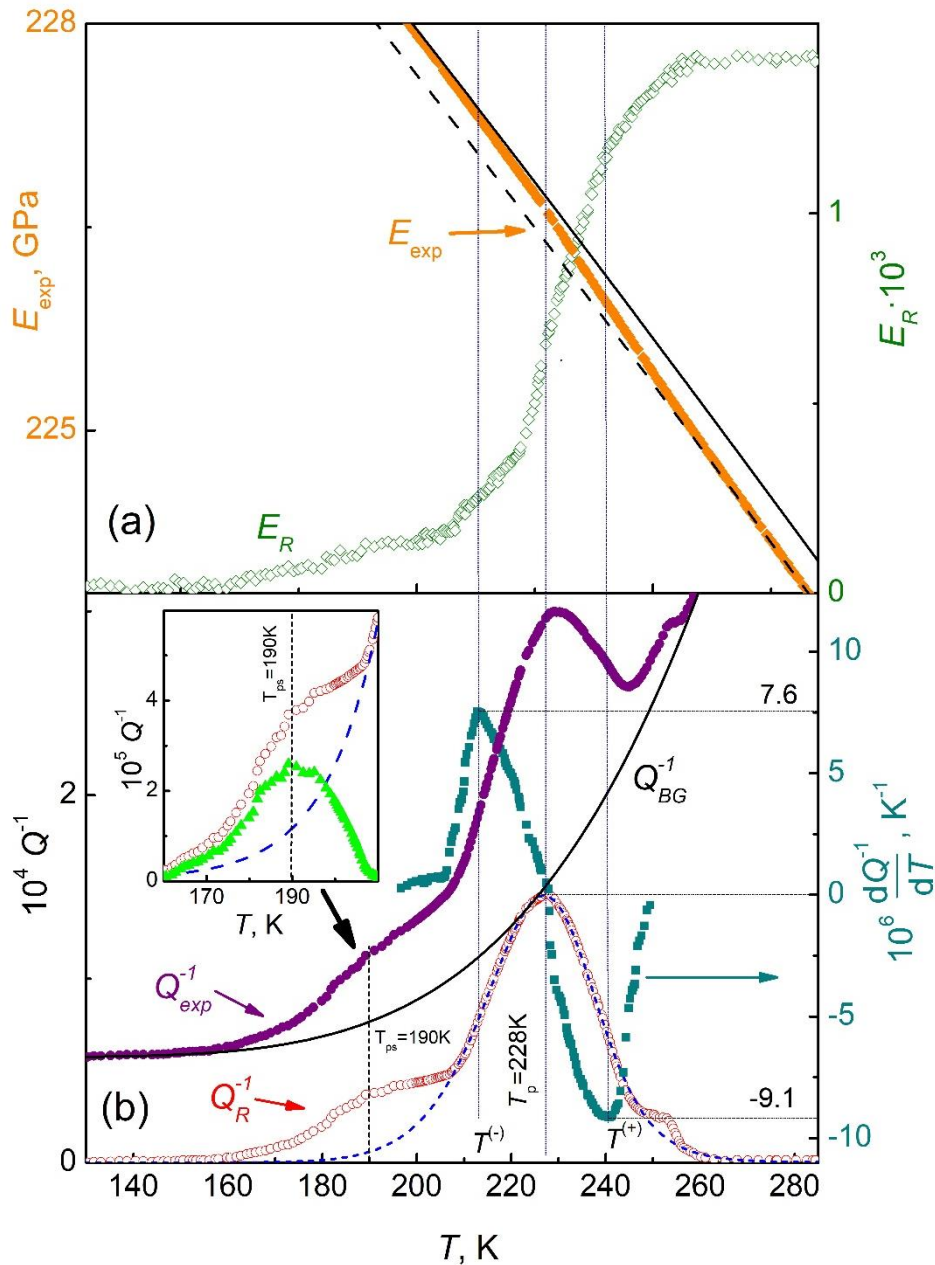


Figure 1. Relaxation resonances in the $\text{Al}_{0.5}\text{CoCrCuFeNi}$ alloy in the structural state (II) [22]: a) temperature dependence of dynamic Young's modulus: \diamond - $E_{\text{exp}}(T)$, \diamond - $E_R(T)$; b) temperature dependence of internal friction: \bullet - $Q_{\text{exp}}^{-1}(T)$, \circ - $Q_R^{-1}(T)$. Solid lines show the background of the dynamic modulus $E_0 - E_{\text{BG}}(T)$ and the absorption background $Q_{\text{BG}}^{-1}(T)$: these graphs are built on the basis of formulas (2) and (6) with the parameter values given in Table. 1. In Figure 2b also shows the results of numerical differentiation of resonant absorption near temperature T_p : \blacksquare - $\frac{\partial}{\partial T} Q_R^{-1}(T, \omega)$. The dotted lines are drawn through the inflection points $T^{(-)}$, $T^{(+)}$ and the

top of the peak T_p , and the dashed line shows the theoretical dependence calculated according to formula (17) with the parameter values given in Table 2.

The inset shows in Figure 1b shows: \circ – resonant component of internal friction $Q_R^{-1}(T)$; the dashed line shows the approximation $\langle Q_R^{-1} \rangle$ for low temperature peak slope $T_p = 228$ K; \blacktriangle – absorption peak satellite $T_{ps} = 190$ K.

We will consider [24] the $Q_{BG}^{-1}(T)$ to be partially caused by thermally activated dislocation relaxation with an activation energy U_{BG} , which differs significantly from the activation energy of the studied resonance absorption. For description $Q_{BG}^{-1}(T)$ we use the relation [27]:

$$Q_{BG}^{-1}(T) = A_1 + A_2 \exp\left(-\frac{U_{BG}}{k_B T}\right). \quad (6)$$

A_1 , A_2 and U_{BG} are fitting parameters. The coefficient A_1 characterizes the contributions to the absorption of the phonon, electronic and magnetic subsystems of the metal, which weakly depend on temperature near resonance.

Relationship (6) well describes the temperature dependence of the acoustic absorption background for state (II) - solid line in Figure 1b (A_1 , A_2 and U_{BG} are given in Table 1).

Table 2. Characteristics of the main absorption peak (a) and its satellite (b) in the state (II).

| (a) | | | | | | |
|----------|-------------|-------------|----------------------|---|---|-------|
| T_p | $T^{(-)}$ | $T^{(+)}$ | $\max Q^{-1}$ | $\max \frac{\partial}{\partial T} \bar{Q}^{-1}$ | $\min \frac{\partial}{\partial T} \bar{Q}^{-1}$ | K |
| 228 K | 213 K | 242 K | $1.5 \cdot 10^{-4}$ | $7.6 \cdot 10^{-6} \text{ K}^{-1}$ | $-9.1 \cdot 10^{-6} \text{ K}^{-1}$ | 0.83 |
| (b) | | | | | | |
| T_{ps} | $T_s^{(-)}$ | $T_s^{(+)}$ | $\max Q_s^{-1}$ | $\max \frac{\partial}{\partial T} \bar{Q}_s^{-1}$ | $\min \frac{\partial}{\partial T} \bar{Q}_s^{-1}$ | K_s |
| 190 K | 182.6 K | 202.0 K | $2.64 \cdot 10^{-5}$ | $3.1 \cdot 10^{-6} \text{ K}^{-1}$ | $-2.5 \cdot 10^{-6} \text{ K}^{-1}$ | 1.24 |

The temperature dependence $Q_R^{-1}(T, \omega)$ of the alloy under study in state (II), after subtracting the background $Q_{BG}^{-1}(T)$, is shown in Figure 1b. Analysis of the temperature dependence of the derivative $\frac{\partial}{\partial T} Q_R^{-1}(T, \omega)$ makes it possible to clarify the peak temperature T_p , obtain the values of the coordinates of the inflection points $T^{(-)}$ and $T^{(+)}$ on the graph $Q_R^{-1}(T, \omega)$ (see Figure 1b), and also estimate the value of the ratio

$$K = \frac{\max \frac{\partial}{\partial T} Q_R^{-1}(T, \omega)}{\left| \min \frac{\partial}{\partial T} Q_R^{-1}(T, \omega) \right|} \quad (7)$$

Registration in experiments of the characteristics of acoustic relaxation resonance T_p , $T^{(-)}$, $T^{(+)}$, $\max Q_R^{-1}$, E_{R0} and K (see Table 2) allows us to formulate a microscopic model of the relaxer and obtain estimates for its parameters [24,28].

However, the resonant component of acoustic relaxation in state (II) is not limited only to the contributions of relaxers responsible for the appearance of the peak $T_p = 228$ K. Figure 1b shows that the resonant component $Q_R^{-1}(T, \omega)$ contains another relaxation resonance, localized on the left slope of the peak $T_p = 228$ K - a satellite $T_{ps} = 190$ K. Its characteristics were obtained further after a detailed analysis of the main peak.

3.2. Mechanical Properties

Mechanical tests of alloy were carried out in the temperature range $0.5 \text{ K} < T < 300 \text{ K}$. The technique for studying mechanical properties by the method of active deformation at a constant rate is described in [21].

The experimental results for both structural states (I) and (II) are shown in Figure 2 with a series of compression deformation diagrams $\tau(\varepsilon; T)$ in the coordinates "shear stress τ - strain ε " at a given strain rate $\dot{\varepsilon} = 4 \cdot 10^{-4} \text{ s}^{-1}$.

It was previously established that the plastic deformation of the alloy under study is determined by the conservative movement of complete dislocations in the $\{111\} <110>$ slip systems, which is typical of fcc crystals (see Figure 5).

Deformation diagrams in Figure 2 at $\varepsilon < 0.1$ have a three-stage shape, typical of metallic polycrystals, in which the lattice symmetry of individual grains allows the existence of easy slip systems. Uniaxial compressive or tensile deformation of such materials begins from the elastic stage,

according to Hooke's law $\tau(\varepsilon) = E\varepsilon$ и $\frac{d\tau(\varepsilon)}{d\varepsilon} = E$. The second stage is the beginning of plastic

deformation in grains that are most favorably oriented with respect to the direction of the deforming stress, with the gradual involvement of other grains in this regime and a decrease in the derivative

$\frac{d\tau(\varepsilon)}{d\varepsilon} < E$. The third stage is plastic deformation of all grains in a stationary mode with a steady-

state value $\frac{d\tau(\varepsilon)}{d\varepsilon} = \text{const} \ll E$, it is called the "stage of linear strain hardening".

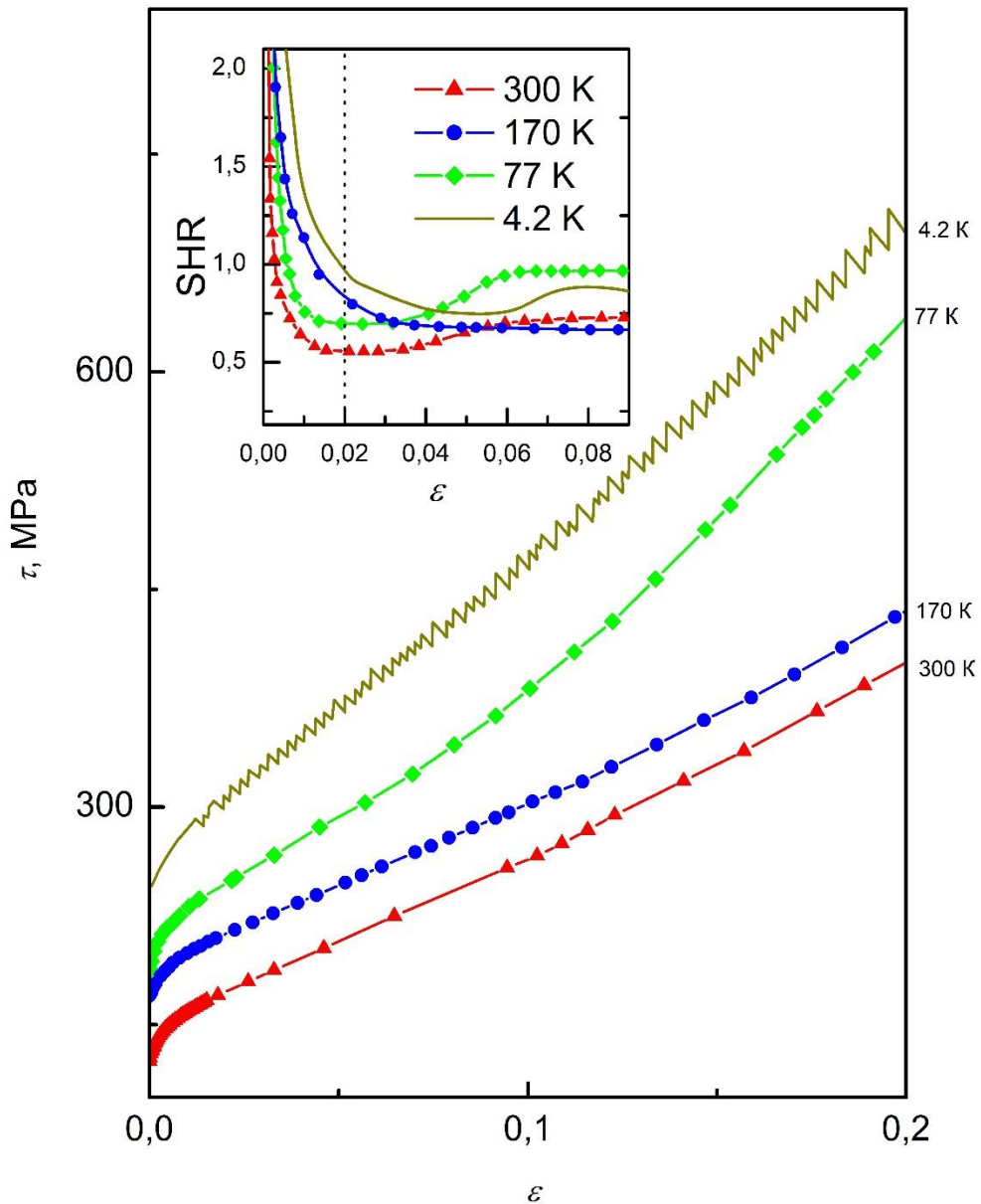


Figure 2. Diagrams of compression deformation of the alloy $\text{Al}_{0.5}\text{CoCrCuFeNi}$ in “ τ - ϵ ” coordinates at different deformation temperatures in structural state (I).

The inset shows the strain-hardening rate (SHR) $\frac{d\tau(\epsilon)}{d\epsilon}$ with deformation ϵ during the low-temperature compression deformation HEA $\text{Al}_{0.5}\text{CoCrCuFeNi}$.

Analysis of the change in the derivative $\frac{d\tau(\epsilon)}{d\epsilon}$ at the initial stages of the deformation diagram showed (inset in Figure 2) that for it the transition from the second to the third stage occurs at $\epsilon \approx 0.02 = 2\%$, therefore for this HEA we will consider stress $\tau_2(T, \dot{\epsilon}) = \tau(\epsilon = 0.02; T, \dot{\epsilon})$ as the yield stress. Figure 3a shows the values $\tau_2(T) = \tau_2(T, \dot{\epsilon} = 4 \cdot 10^{-4} \text{ s}^{-1})$ obtained from the strain diagrams in Figure 2.

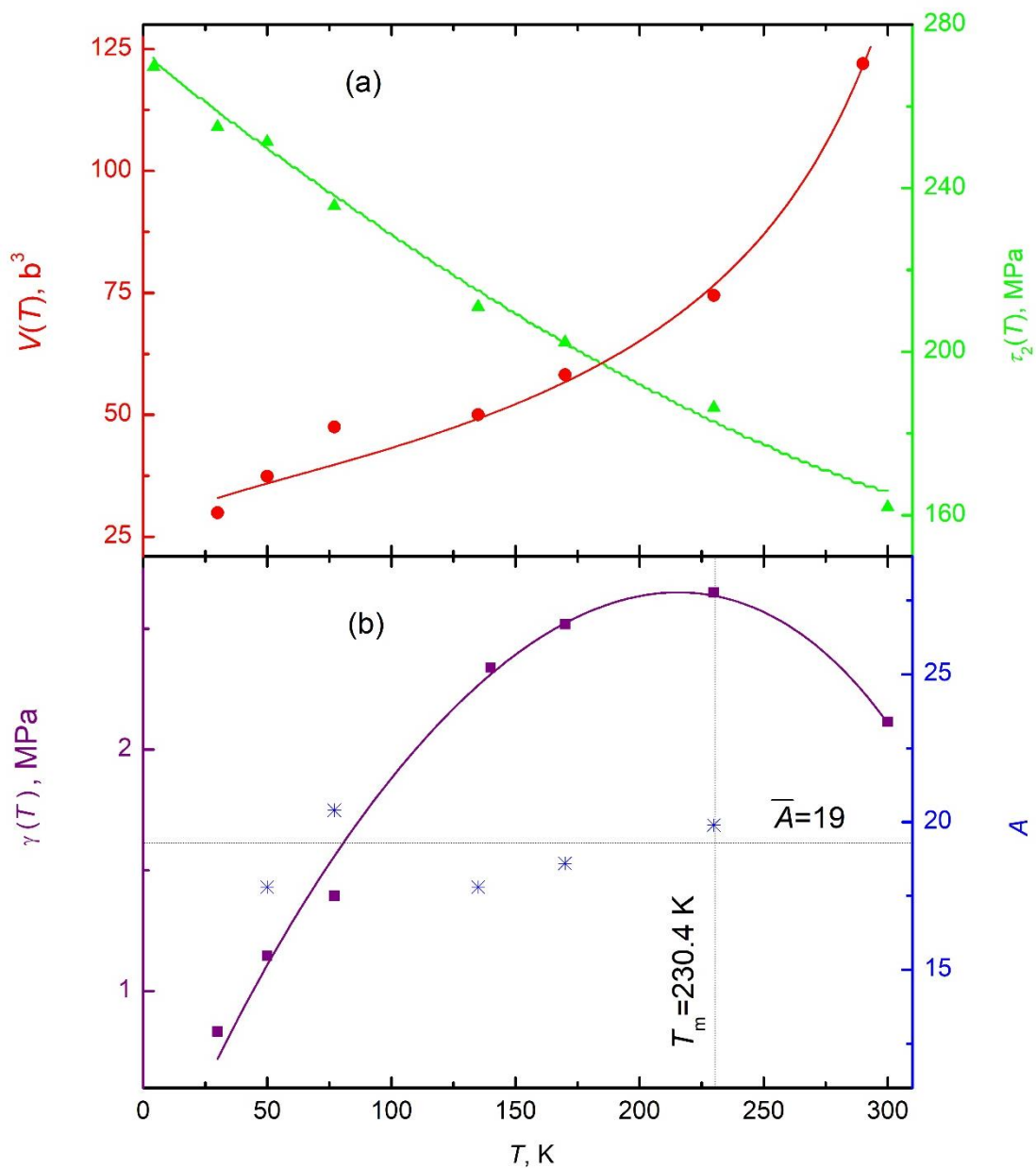


Figure 3. Temperature dependences of plasticity characteristics in state (I) at $\varepsilon = 0.02$: (a) \blacktriangle - yield stress $\tau_2(T)$ and \bullet - activation volume of the plastic deformation process $V(T)$; (b) \blacksquare - speed sensitivity of deformation stress $\gamma(T)$ and $*$ - empirical values of parameter A .

In both figures, solid lines show analytical approximations of experimental points by theoretical formulas (32).

During the process of active deformation at a given temperature, the stress increment $\Delta\tau_2(T)$ was also recorded with the strain rate $\dot{\varepsilon}$ increase by 4.4 times from $4 \cdot 10^{-4}$ s⁻¹ to $1.8 \cdot 10^{-3}$ s⁻¹. At deformation $\varepsilon = 0.02$, the strain rate sensitivity $\gamma(T)$ of the conditional yield strength τ_2 and the activation volume $V(T)$ of the plastic deformation process were determined (Figure 3):

$$\gamma(T) = \frac{\Delta\tau_2(T)}{\Delta \ln \dot{\varepsilon}}, \quad V(T) = kT \frac{\Delta \ln \dot{\varepsilon}}{\Delta\tau_2(T)} = \frac{kT}{\gamma(T)}, \quad \text{where } k \text{ is Boltzmann's constant.} \quad (8)$$

4. Low Temperature Dislocation Processes in HEA Al_{0.5}CoCrCuFeNi

The alloy under study in states (I) and (II) has the morphology of a polycrystalline with an fcc lattice. Therefore, it is natural to assume that the features of the initial stage of plastic deformation and acoustic relaxation resonances in this alloy are due to the dynamics and kinetics of dislocation processes similar to low-temperature dislocation processes in polycrystals of monatomic materials with an fcc structure [24,29–37]. Differences in the atomic structure and morphology of grain boundaries in HEAs and simple metals must be taken into account only when interpreting experimental results obtained under conditions of sufficiently high temperatures, when their acoustic and mechanical properties are significantly influenced by the processes of thermally activated diffusion transformation of grain boundaries of polycrystals, in particular, absorption and generation of dislocations that determine plastic deformation.

The interpretation of the laws of dislocation plasticity and the influence of dislocations on the acoustic properties of metals is based on the idea of the presence of easy slip planes in their structure and the specificity of the nucleation and movement of dislocations in these planes [38,39]. Currently, experimental methods for observing such processes have been developed, as well as theoretical descriptions of the results of these experiments based on concepts of the dynamics and kinetics of thermally activated and quantum motion of dislocations in easy slip planes through various barriers, taking into account their inhibition not only by barriers, but also by quasiparticles - conductivity electrons and phonons [22,24,28].

4.1. Models of Dislocation Relaxers

Let us use the algorithm [24,28] for analyzing mechanical spectroscopy data, which allows us to establish the microscopic mechanism of relaxation resonances and obtain estimates for the parameters of elementary relaxers based on an analysis of the temperature dependences $Q_{\exp}^{-1}(T)$ and $E_{\exp}(T)$ obtained in experiments at one fixed value of the sample oscillation frequency $\omega_r = 2\pi f_r$.

Since the bulk of the samples of the studied alloy, both in state (I) and state (II), consists of a material with an fcc lattice, it is natural to assume that the observed acoustic relaxation resonances in this alloy are determined by mechanisms that are similar to resonances in metals with an fcc structure. Such resonances are interpreted as a consequence of the interaction of elastic vibrations of the sample with a system of dislocation relaxers, since they are observed only after preliminary plastic deformation of the samples. On the temperature dependence of internal friction, they correspond to Bordoni peaks in the range 20 K $< T <$ 100 K [31–34] and Hasiguti peaks in the range 100 K $< T <$ 200 K [40]. The positions of these peaks $T_p(\omega)$ on the temperature axis depend on the vibration frequency ω and differ for different metals.

In fcc crystals at the initial stage of deformation, dislocation plastic sliding predominantly occurs along close-packed <110> directions and {111} planes (Figure 4). In the {111}<110> slip system, there are two types of rectilinear dislocations with the Burgers vector \mathbf{b} whose lines D^{qe} and D^s are oriented along the directions ox of dense packing. But for D^{qe} the vector \mathbf{b}^{qe} has a quasi-edge (close to the edge) orientation, and for D^s the vector \mathbf{b}^s has a purely s screw orientation: the angle between the vector \mathbf{b}^{qe} and the unit τ of the dislocation line has the value $\alpha = 60^\circ$, and the angle between \mathbf{b}^s and τ is equal to zero, while $|\mathbf{b}^{qe}| = |\mathbf{b}^s| = |\mathbf{b}| = \frac{\sqrt{3}}{2} = a_0$, a_0 is the distance between the nearest nodes.

Moving lines in the transverse direction The movements of rectilinear dislocation lines in the transverse direction OZ are controlled by the first kind Peierls lattice potential relief with period

a_{p1} , but the height of the barriers of this relief and the corresponding Peierls critical stress values τ_{p1}^s and τ_{p1}^{qe} for pure screw dislocations are significantly greater than for quasi-edge ($\tau_{p1}^s \gg \tau_{p1}^{qe}$).

When such dislocations nucleate and move in real materials with structural defects on the surface and in the bulk, the formation of only straight configurations of dislocation lines is unlikely [41]. At the early stages of plastic deformation, a set of curved dislocation segments is formed (see Figure 5) with *ABC* configurations between the attachment points, which consist of shorter fragments *AB* and *BC* with significantly different crystal geometric and dynamic properties. Straight-line segments of the dislocation line *BC* with a length L are oriented along the directions of dense packing and are located in the valleys of the Peierls relief, and fragments *AB* with a length \tilde{L} consist of chains of kinks connecting short straight-line segments of dislocation lines in neighboring valleys of the relief. The self-energy of an individual kink also has a periodic component if its center x_k moves along the direction of close packing parallel to the axis *OX*: this is called the secondary Peierls relief. The period of this relief is equal to the minimum distance between nodes $a_{p2} = a_0$, and the height of the barriers and the values of critical stresses τ_{p2}^s and τ_{p2}^{qe} are different for D^{qe} and D^s dislocations ($\tau_{p2}^s \ll \tau_{p2}^{qe}$). The *ABC* segment has the properties of a two-mode dislocation relaxer, which consists of fragments L and \tilde{L} . The significant difference in the crystal geometric and energy characteristics of the fragments also determines the difference in the dynamic and relaxation properties of these components L and \tilde{L} of the relaxer during its interaction with elastic vibrations of the sample.

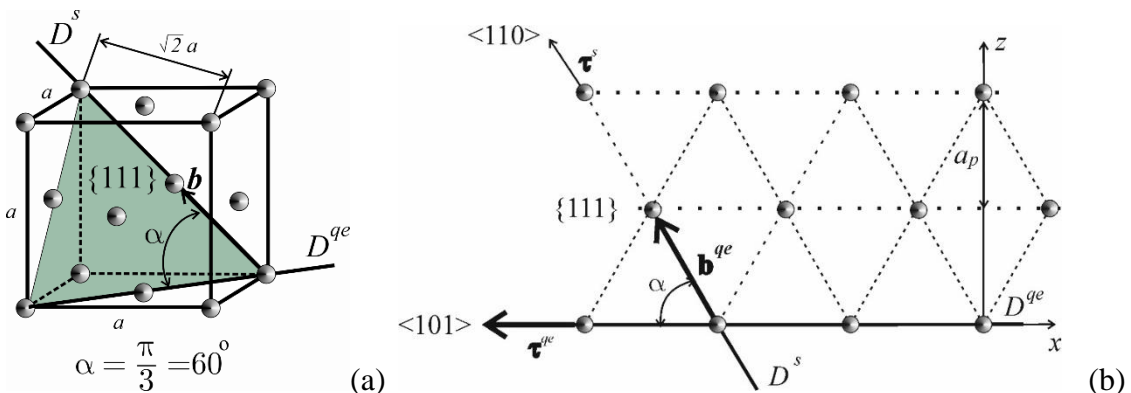


Figure 4. $\{111\}\langle 110 \rangle$ slip system and straight dislocations in an fcc crystal: (a) – unit cell; (b) – one of the sliding planes $\{111\}$.

●, a - nodes and fcc lattice parameter, $a = 0.36$ nm [6]; D^{qe} , D^s – lines of quasi-edge and screw dislocations with a common Burgers vector $\mathbf{b}^{qe} = \mathbf{b}^s = \mathbf{b} = b\langle 0\bar{1}\bar{1} \rangle$ with length $b^s = b^{qe} = b = a_0 = \frac{a}{\sqrt{2}}$, $b = 0.254$ nm [13]; $a_p = \frac{\sqrt{3}}{2}a_0 = \frac{\sqrt{3}}{8}a$ - Peierls relief period in the direction of easy sliding; a_0 - distance between adjacent nodes in the direction of easy sliding.

It is known that the elementary relaxers for the Bordoni and Hasiguti peaks are fragments of dislocation lines in easy slip systems $\{111\}\langle 110 \rangle$ of fcc metals, which are excited by elastic vibrations [37,40]. In the proposed model of a two-mode dislocation relaxer, the role of such fragments is played by its components *BC* (length L) and *AB* (length \tilde{L}). It is assumed that their

ends A , B and C are fixed by local defects in the lattice structure, which prevent the movement of the dislocation line in the slip plane.

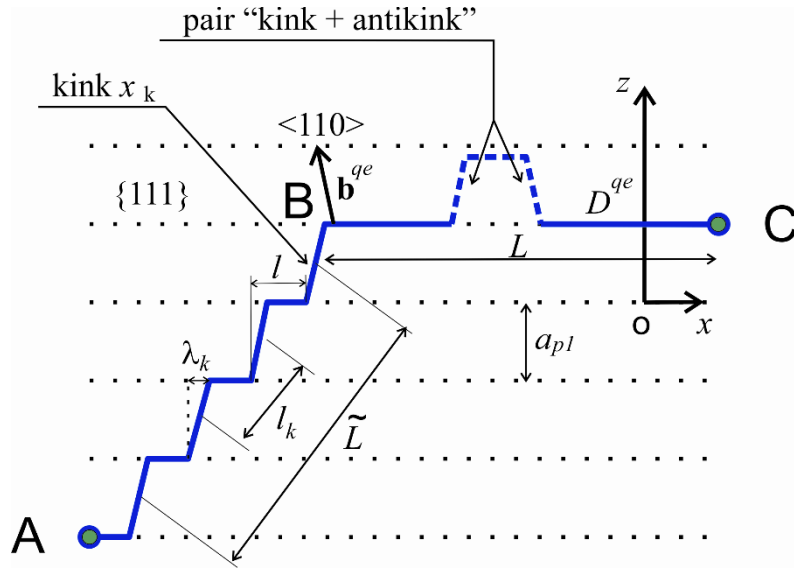


Figure 5. Configurations of dislocation lines in the $\{111\}<110>$ slip system in an fcc crystal: ABC – curved segment of a quasi-edge dislocation D^{qe} with a Burgers vector \mathbf{b}^{qe} , the dotted line indicates the close packing directions; a_{p1} – period of the first kind Peierls relief in the direction of the axis OZ ; $a_0=b$ – period of secondary Peierls relief; L – length of straight segment BC in the relief valley; \tilde{L} – length of the chain of AB kinks between relief valleys; x_k – coordinate of a separate kink along the axis OX ; λ_k – kink width; l – distance between the centers of neighbouring kinks.

Bordoni peaks were interpreted by Seeger [35–37] as a result of thermally activated nucleation of paired kinks on straight segments of dislocation lines L located in the valleys of the Peierls relief (Figure 6a).

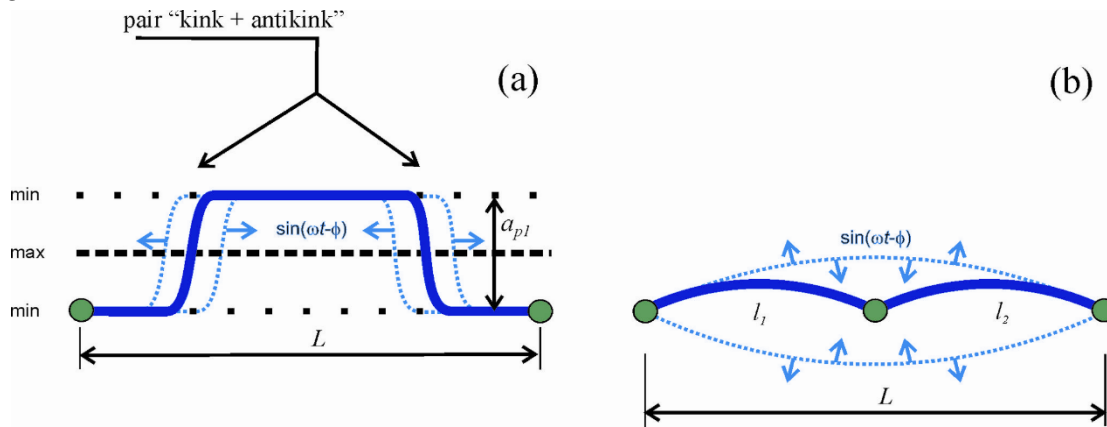


Figure 6. Schematic representation of an elementary relaxer: (a) – Seeger relaxation; (b) – relaxation Koiwa and Hasiguti; ● – local defects on the dislocation string; the symbol L denotes the length of the dislocation segment, the activation of which determines the elementary contribution of the dislocation to the acoustic resonance or the rate of plastic deformation.

For Hasiguti peaks, Koiwa and Hasiguti [40] considered the thermally activated detachment of a dislocation line segment $L = l_1 + l_2$ from an individual point defect (impurity atom, vacancy, radiation defect, etc.) as an elementary relaxation process (Figure 6b). It has been established that

vibrations of a chain of geometric kinks on a segment of a dislocation line with fixed ends are described by the equation of vibrations of a segment of a dislocation string [39,41].

4.2. Thermal Activation and Statistical Analysis of the Dislocation Contribution to Acoustic Relaxation

A separate elementary statistically independent process of thermally activated excitation of a dislocation relaxer is characterized by a relaxation time, which depends on temperature according to the Arrhenius law:

$$\theta(T) = \theta_0 \exp\left(\frac{U_0}{k_B T}\right) \quad (9)$$

U_0 (activation energy) and θ_0 (effective period of attempts) are determined by the crystal geometric and energy characteristics of a particular relaxer in a particular crystal. The θ_0 has a weak power-law dependence on temperature, which can be neglected against the background of the exponential dependence of the second factor at low temperatures $kT \ll U_0$.

The temperature-frequency dependence of internal friction, caused by a system of relaxers with the same values of parameters U_0 and θ_0 , is described by the formula

$$Q_R^{-1}(T, \omega) = C_r \Delta_0 F(\omega \theta) \quad (10)$$

Here Δ_0 and C_r are, respectively, the effective specific contribution of an individual relaxer and their concentration, and $F(\omega \theta)$ is a positive definite function with a sharp maximum at $\omega \theta \approx 1$. The form of the function $F(\omega \theta)$ and the position of its maximum on the temperature axis $T_p(\omega)$ depend on the nature of the relaxers. Most of them belong to the class of Debye relaxers, for which thermal activation occurs simultaneously in the forward and reverse directions with respect to the exciting voltage; the Seeger relaxation meets this criterion and is a special case of the Debye relaxation. But in the Koiwa-Hasiguti process, thermal activation stimulates the excitation of relaxers only in the forward direction, and their return to the initial unexcited state occurs under the action of the linear tension force of the dislocation segments. This results in two different expressions for the function $F(\omega \theta)$ [28,40]:

$$F^D(x) = \frac{x}{1+x^2}, \quad F^{K-H}(x) = \frac{x^2}{2(1+x^2)} \left[1 - \exp\left(-\frac{2\pi}{x}\right) \right], \quad x = \omega \theta \quad (11)$$

For relaxation processes of both types, the function $F^{D,K-H}(x)$ vanishes at $x \rightarrow 0$ and $x \rightarrow \infty$, but has a sharp maximum at $x_m^D = 1$ and $x_m^{K-H} = 2.67$, respectively. If the value of the oscillation frequency ω is fixed, then for a system of identical relaxers with parameters U_0 and θ_0 internal friction $Q_R^{-1}(T, \omega)$ on the temperature axis has a sharp maximum (peak) at temperature $T_p^{D,K-H}(\omega)$:

$$T_p^{D,K-H}(\omega) = \frac{U_0}{k_B \alpha^{D,K-H}}; \quad \alpha_D = -\ln \omega \theta_0, \quad \alpha_{K-H} = -\ln \frac{\omega \theta_0}{2.67} \approx 1 - \ln \omega \theta_0 \quad (12)$$

Parameter estimates obtained U_0 , θ_0 , $C_r \Delta_0$:

- for Seeger relaxers

$$U_0 \sim 0.1 \text{ eV}, \quad \theta_0 \sim 10^{-11} \text{ s and } C_r \Delta_0 \sim 10^{-1} \rho_L L^3, \quad (13)$$

where L is the length of a straight dislocation segment in the Peierls relief valley, and ρ_L is the number of such segments per unit volume;

- for Koiwa-Hasiguti relaxers

$$U_0 \sim (0.3 \div 0.5) \text{ eV}, \theta_0 \sim 10^{-13} \text{ s and } C_r \Delta_0 \sim 10^{-1} \rho_L L^3, \quad (14)$$

where L and ρ_L are, respectively, the length and volume density of dislocation segments breaking away from an individual point defect.

The action of the relaxation process is accompanied by a decrease in the dynamic modulus of elasticity by the amount $E_R(T, \omega) = E_R(\omega\theta)$. In this case $E_R(\omega\theta \rightarrow \infty) = 0$, and a decrease of $\omega\theta$ leads to a monotonic increase $E_R(T, \omega)$ to $E_{R0} = E_R(\omega\theta \rightarrow 0)$.

Let us note two differences between the Debye and Koiwa-Hasiguti processes:

- in [24] it is shown that these processes correspond to different values of the ratio of the peak height $\max Q_R^{-1}(\omega\theta)$ to the step height $E_{R0} = E_R(\omega\theta \rightarrow 0) - E_R(\omega\theta \rightarrow \infty)$ on the temperature-frequency dependences of the contributions of these relaxation processes to the internal friction and dynamic elasticity of materials:

$$\left[\frac{E_0}{E_{R0}} \cdot \max Q_R^{-1} \right]^D = 0.5, \quad \left[\frac{E_0}{E_{R0}} \cdot \max Q_R^{-1} \right]^{K-H} \approx 0.13 \quad (15)$$

- in [28] it was established that the parameter K determined by relation (7) does not depend on temperature and U_0 , and its frequency dependence is described by monotonic functions

$K = K_{D,K-H}(\omega\theta_0)$, while:

$$K_D(\omega\theta_0) > 1.2, \quad K_{K-H}(\omega\theta_0) < 1.2, \quad \omega\theta_0 < 10^{-3} \quad (16)$$

Relations (9)-(16) describe the acoustic relaxation resonance in an ideal crystal, caused by a system of similar dislocation relaxers with the same values of the parameters of an individual relaxer U_0 , θ_0 and Δ_0 . In a real HEAs, there is a complex system of random structural defects or inhomogeneities and the internal stress fields they create. Therefore, the parameters of the same type relaxers U_0 , θ_0 and Δ_0 acquire random additives in different areas of the sample, which leads to a statistical broadening of peaks and steps in the dependence graphs $Q_R^{-1}(T, \omega)$ and $E_R(T, \omega)$; and also to a shift in the temperature $T_p(\omega)$ of their localization. In HEAs, random inhomogeneities are associated not only with the chaotic distribution of defects, but also with distortions of unit cells in the crystal lattice by random configurations of alloy components and differences in their atomic radii [42].

Following [24,28], we will consider U_0 , θ_0 and Δ_0 as random variables with their corresponding distribution patterns. But at low temperatures $k_B T \ll U_0$ it is enough to take into account only statistical deviations of the activation energy U from U_0 and with exponential accuracy we can neglect the scatter of parameters θ_0 and Δ_0 . In this case, the contribution of relaxers to internal friction $\langle Q_R^{-1}(T, \omega) \rangle$ and dynamic modulus of elasticity $\langle E_R(T, \omega) \rangle$ will be determined by averaging the initial formulas for the dependencies $Q_R^{-1}(T, \omega)$ and $E_R(T, \omega)$

with a quasi-Gaussian distribution function $P(U; U_0, D)$ for the activation energy, in which the role of parameters is played by activation energy U_0 and its dispersion characteristics D [22,24,28].

After averaging, relation (10) takes the form:

$$\langle Q_R^{-1} \rangle = Q_R^{-1}(T, \omega; \theta_0, U_0, D) = C_r \Delta_0 \int_0^{\infty} dU P(U; U_0, D) F^{D, K-H}(\omega \theta), \quad (17)$$

The statistical spread of activation energy does not affect the form of functions $K_{D, K-H}(\omega \theta_0)$ and preserves (16), which allows us to establish a physical model of a dislocation relaxer.

The statistical spread of activation energy leads to a decrease in the height of the internal friction peak $\max \langle Q_R^{-1} \rangle < \max Q_R^{-1}$ and an increase in its width; and also increases the width of the step on the temperature dependence of the module $\langle E_R(T, \omega) \rangle$, but maintains its height E_{R0} . Therefore, at a small value of the parameter $D \ll U_0$, relations (15) are approximately preserved and can be used to select a relaxer model.

4.3. Dislocation Mechanism of the Internal Friction Peak $T_p = 228$ K (Analogue of the Hasiguti Peak)

Comparing the resonance parameters (Table 2) near temperature $T_p = 228$ K with relations (15) and (16), we come to the conclusion that it corresponds to the Koiwa-Hasiguti process, i.e. thermally activated separation of dislocation segments from point defects:

$$K = 0.83 < 1.2, \quad \frac{E_0}{E_{R0}} \cdot \max Q_R^{-1} \approx 0.1$$

In the studied alloy, the role of point defects can be played by nanoclusters of several atoms of one of the chemical elements of the alloy (3) or traditional point defects of the crystal structure - vacancies and interstitial atoms. Therefore, for a theoretical description of resonance, we use (17), assuming that $F(\omega \theta) = F^{K-H}(\omega \theta)$, and in the future we will omit the index "K-H". In [6], relations were obtained that allow one to estimate the values of the parameters U_0 , θ_0 , Δ_0 and D if we use the experimentally recorded values of the resonance characteristics T_p , $T^{(-)}$, $T^{(+)}$, $\max Q_R^{-1}$, E_{R0} and K (see Table 2):

$$(\alpha - 1)^{1,43} = \frac{10}{K - 0,7}, \quad \omega \theta_0 = \exp(1 - \alpha); \quad C_r \Delta_0 = 2.5 \max Q_R^{-1} \cdot \exp\left(\frac{7\sqrt{2}\alpha D}{56\sqrt{2}D + 20U_0}\right) \quad (18)$$

$$U_0 = 8k_B \alpha^2 \cdot (2T_p - T^{(-)} - T^{(+)}) , \quad D = \frac{20k_B \alpha}{11\sqrt{2}} \cdot (9T^{(+)} + 10T^{(-)} - 19T_p) \quad (19)$$

Substituting into (18) and (19) the values of the resonance characteristics from Table 2 we obtain estimates for the relaxer parameters U_0 , Δ_0 and θ_0 (Table 3), which allows us to calculate the theoretical profile $\langle Q_R^{-1} \rangle$ of the internal friction peak (solid line in Figure 7).

The obtained values of activation energy $U_0 \approx 0.4$ eV and effective oscillation period $\theta_0 \approx 10^{-13}$ s are typical for Koiwa-Hasiguti relaxers in simple metals with an fcc structure. A small value $D \sim 10^{-2} U_0$ indicates the absence of significant structural distortions in state (II), which is due to long-term annealing, which was used to form this structural state.

Table 3. Parameters of dislocation relaxers for the peak of internal friction T_p and its satellite T_{ps} .

| θ_0 | U_0 | D | $C_r \Delta_0$ | θ_0^s | U_0^s | D^s | $C_r^s \Delta_0^s$ |
|----------------------|---------|---------|-------------------|----------------------|---------|---------|--------------------|
| $2 \cdot 10^{-13}$ s | 0.43 eV | 0.01 eV | $4 \cdot 10^{-4}$ | $4 \cdot 10^{-11}$ s | 0.07 eV | 0.01 eV | $1 \cdot 10^{-4}$ |

Using (14) and assuming $C_r \approx \rho_L$ we obtain an estimate $\Delta_0 \sim 10^{-1} L^3$ for the contribution of one relaxer to internal friction and decreasing of the elastic modulus. Let us assume that the role of local centers of pinning of dislocation segments is played by small atomic clusters with a distance between them of the order of several nanometers: they are recorded in state (II) by electron microscopy methods [23]. Then, when estimating the length L , we can take twice the distance between clusters $L \sim 10$ nm, and given in Table 2 corresponds to the volume density of relaxers $C_r = \rho_L \sim 4 \cdot 10^{21}$ m⁻³. For the dislocation density $\Lambda_d = l \rho_L$ (total length of dislocation segments per unit volume), which effectively interact with elastic vibrations of the sample, we obtain the estimate $\Lambda_d \sim 4 \cdot 10^{13}$ m⁻².

4.4. Dislocation Mechanism of Internal Friction Peak $T_{ps} = 190$ K (Analogue of Bordoni Peak)

A satellite peak with a maximum at $T_{ps} = 190$ K is observed on the low-temperature branch of the main peak $T_p = 228$ K. To isolate it and subsequent analysis, it is necessary to subtract the contribution of theoretical dependence $\langle Q_R^{-1} \rangle$ from the experimentally observed relaxation $Q_{\text{exp}}^{-1}(T)$ at the values of the relaxator parameters U_0 , θ_0 and Δ_0 corresponding to the main peak (Table 3). The results of this procedure are shown in the inset in Figure 1b.

Using the statistical and thermal activation analysis described above, we come to the conclusion that the peak $T_{ps} = 190$ K is due to Seeger relaxation, and the estimates for its parameters are given in Table 3.

We will carry out a theoretical description of the movement of a dislocation line in a first kind Peierls relief in the case of a sinusoidal relief, when the linear energy density $W(z_d)$ of an element of a dislocation line has the form:

$$W(z_d) = \Gamma + W_0 \sin^2 \frac{\pi z_d}{a_p} - b \sigma z_d, \quad W_0 = \frac{ba_p}{\pi} \tau_{p1} \quad (20)$$

here Γ is the energy per unit length of a dislocation in the continuum approximation (linear tension); W_0 and τ_{p1} - magnitude of barriers and critical stress for Peierls relief of the first type; $\tau = \tau_{xz}$ - shear stress component in the slip plane; z_d - coordinate of the dislocation line element along the axis oz (Figure 5).

The equation of motion of a string with linear mass density M in the potential (20) has soliton solutions in the form of kinks, and their characteristics are related to the parameters of the potential and dislocation by the formulas [24]:

$$\lambda_k = a_p \sqrt{\frac{2\Gamma}{\pi ba_p \tau_{p1}}}, \quad m_k = \frac{2a_p M}{\pi} \sqrt{\frac{2ba_p \tau_{p1}}{\pi \Gamma}}, \quad \varepsilon_k = m_k c_t^2, \quad \theta_{p1} = \frac{\pi \lambda_k}{c_t}, \quad c_t = \sqrt{\frac{\Gamma}{M}}. \quad (21)$$

Here λ_k , m_k , ε_k are the width, mass and energy of the kink, respectively, θ_{p1} is the period of natural oscillations of a rectilinear segment in the relief valley, c_t is the characteristic value of the speed of transverse sound vibrations in the crystal.

The average time of thermally activated nucleation of kink-antikink pairs on a straight segment of a dislocation line (Figure 6a) is described by the Arrhenius law (9) with activation energy $U \approx 2\varepsilon_k$ and attempt period $\theta_0 \approx \theta_{p1}$. The interaction of elastic vibrations $\tau \ll \tau_{p1}$ with such a process is one of the mechanisms of relaxation resonance [31]. If the sample contains the volume density ρ_L of straight dislocation segments with length L , then their contribution to the dynamic modulus of elasticity and vibration decrement is described, without taking into account the statistical scatter of parameters, by formulas (9)-(12), in which

$$U = U_0 \approx 2\varepsilon_k, \quad \theta_0 = \theta_{p1}, \quad (22)$$

We assume that the discussed resonance $T_{ps} = 190$ K in the studied HEA is caused by the Seeger process, therefore, according to (13)

$$C_r \Delta_0 = (C_r \Delta_0)_L \approx 10^{-1} L^3 \rho_L. \quad (23)$$

Comparison of the values of parameters U_0^s and θ_0^s obtained as a result of the analysis of experimental data (see Table 3) with the formulas of the theory (20)-(23) does not lead to contradictions and allows us to obtain estimates for the characteristics of dislocations responsible for resonance.

From (21) and (22) the next relations follow:

$$U_0 = 2c_t^2 m_k, \quad \frac{U_0}{\theta_{p1}} = \frac{4c_t b a_p}{\pi^2} \tau_{p1}, \quad U_0 \theta_{p1} = \frac{8a_p^2}{\pi} \sqrt{\Gamma M} = \frac{8a_p^2}{\pi c_t} \Gamma = \frac{8c_t a_p^2}{\pi} M \quad (24)$$

The necessary for further assessments parameters of the studied HEA have the following values:

$$b = a_0 = 2.54 \cdot 10^{-10} \text{ m}, \quad a_p = \frac{\sqrt{3}}{2} a_0 \approx 0.87 a_0 \approx 2.2 \cdot 10^{-10} \text{ m} \quad [29];$$

$$\rho = 7.98 \cdot 10^3 \frac{\text{kg}}{\text{m}^3} \quad [22](6), \quad G = \frac{E}{2(1+\nu)} = 0.94 \cdot 10^{11} \text{ Pa}, \quad c_t = \sqrt{\frac{G}{\rho}} \approx 3.4 \cdot 10^3 \frac{\text{m}}{\text{s}} \quad (25)$$

here G - shear modulus, Poisson's ratio $\nu \approx 0.22$ [49], ρ - density. The resulting estimate $c_t = \sqrt{\frac{G}{\rho}} \approx 3.4 \cdot 10^3 \frac{\text{m}}{\text{s}}$ is in good agreement with the data [49].

Substituting into (21) -(24) the values of the activation energy $U_0 = U_0^s \approx 11.2 \cdot 10^{-21} \text{ J}$, the period of attempts $\theta_0^s \approx 4 \cdot 10^{-11} \text{ s}$ and $(C_r \Delta_0)_L \leq 1 \cdot 10^{-4}$ for resonance $T_{ps} = 190$ K leads to the following estimates for the parameters of the dislocation model under consideration:

$$m_k \approx 5 \cdot 10^{-3} m_a \approx 5 \cdot 10^{-28} \text{ kg}, \quad \lambda_k \approx 40 a_0 \approx 1 \cdot 10^{-8} \text{ m}, \quad \tau_{p1} \approx 3.6 \cdot 10^6 \text{ Pa} \approx 4 \cdot 10^{-5} G, \\ M \approx 1.1 \cdot 10^{-15} \frac{\text{kg}}{\text{m}} \approx 2.1 \rho b^2, \quad \Gamma \approx 12.4 \cdot 10^{-9} \frac{\text{J}}{\text{m}} \approx 2.1 G b^2, \quad \rho_L L^3 \leq 10^{-3}. \quad (26)$$

Here the mass m_k and width λ_k of the kink are compared with the average mass m_a of an atom of the studied alloy and the minimum interatomic distance a_0 , and the Peierls critical stress τ_{p1} with the shear modulus G .

The good correspondence of the estimates for the parameters Γ and M with their estimates $\Gamma \approx G b^2$ and $M \approx \rho b^2$ in the continuum theory of dislocations is a serious argument in favor of

the adequacy of the proposed model of the relaxation process $T_{ps} = 190$ K to the experimentally recorded resonance properties.

4.5. Dislocation Processes of Low-Temperature Plastic Deformation

In the previous sections, an analogy was established and described between elementary dislocation processes that determine low-temperature acoustic resonances of simple polycrystalline metals with an fcc atomic structure and HEA $\text{Al}_{0.5}\text{CoCrCuFeNi}$ - thermal excitation of components on two-mode dislocation relaxators in an easy slip system $\{111\}\langle 110 \rangle$. It is assumed that such two-mode relaxers (Figure 6) are formed in polycrystal grains during its preparation and primary processing of samples. It is natural to assume that in order to interpret the results of low-temperature mechanical tests of HEA $\text{Al}_{0.5}\text{CoCrCuFeNi}$ within the framework of dislocation concepts, the use of this analogy will also be appropriate and effective.

In modern physics of low-temperature plasticity [43], one of the central tasks is to elucidate the relative role of Peierls relief and local barriers (impurity and intrinsic interstitial atoms, vacancies and a number of other violations of the atomic structure with dimensions of atomic scales) in the processes of movement of dislocations. When studying this problem, the ultimate goal is to interpret the yield stresses and the initial stages of plastic deformation.

During low-temperature deformation of pure bcc metals in the stationary easy slip mode, it was established [44] that the kinetics of deformation is determined by the movement of dislocations in the $\{110\}$ planes of the bcc structure through Peierls barriers according to the mechanism of nucleation and expansion of pair kinks as a result of the action of thermal or quantum fluctuations (scheme of such a process shown in Figure 6a). This mechanism corresponds to a large value of the yield stress $\approx 10^{-3} G$ and its sharp increase with decreasing temperature, and the dependence shows a characteristic feature during the transition from small to large values of deforming stress, due to a change in the law of interaction of kinks. Impurity interstitial atoms at concentrations above 0.7 at. % have a noticeable effect on the magnitude and temperature dependence of the yield stress of these metals [45].

In simple fcc metals, Peierls barriers in the easy slip plane $\{111\}$ are negligible and the yield stress is $\leq 10^{-5} G$, and the main obstacles to dislocation glide are local barriers created by substitutional impurities, which are overcome by dislocation strings due to thermal or quantum fluctuations (a diagram of such a process is shown in Figure 6b). Substitutional impurities in fcc metals are relatively weak barriers to dislocations; therefore, this mechanism corresponds to a less sharp increase in the yield strength when cooling samples than in the case of pure bcc metals.

At high concentrations of impurities (1 at.% and higher), the yield strength of simple fcc metals increases more sharply upon cooling and can acquire a characteristic low-temperature anomaly - a maximum in the dependence of the conditional yield strength, which arises due to the transition from a purely fluctuational to a fluctuation-inertial mechanism of dislocation motion through impurity barriers (unzipping effect) [43,46,47]. In this case, the $\tau_{0.2}$ decreases with decreasing temperature since some of the local obstacles are overcome by dislocations without activation. The condition for the inertial movement of dislocations is a high effective stress $\tau^*(T) = \tau - \tau_i$ (τ - deformation stress, $\tau_i = \tau_i(\varepsilon; T)$ - long-range internal stress) and a low coefficient of dynamic friction of dislocations.

To describe the kinetics of plastic deformation during purely thermally activated stationary motion of dislocations through a system of similar local obstacles, the Arrhenius relation is used, which determines the exponential dependence of the strain rate $\dot{\varepsilon}$ on the deforming stress τ and temperature T :

$$\dot{\varepsilon} = \dot{\varepsilon}_0 \exp\left[-\frac{H(\tau^*)}{kT}\right], \quad \tau^* = \tau - \tau_i(\varepsilon; T). \quad (27)$$

Here $\dot{\varepsilon}_0$ is the pre-exponential factor, proportional to the frequency θ_0^{-1} of attempts to overcome obstacles and the volume density of elementary independent structural units, the activation of which determines the kinetics of the process (Figure 7), and $H(\tau^*)$ is the effective energy (enthalpy) of activation. It is assumed that the power-law dependence $\dot{\varepsilon}_0$ on stress and temperature in a purely thermally activated mode of dislocation motion is insignificant against the background of the exponential dependence of the second factor in (27). This dependence should be taken into account only when transitioning to the thermoinertial mode of dislocation motion, taking into account the unzipping effect.

The dependence $H(\tau^*)$ is determined by the force law of interaction of a dislocation with the center of pinning (obstacle), as well as the statistics of the distribution of obstacles along the dislocation. In most cases [45] :

$$H(\tau^*) = H_0 \left[1 - \left(\frac{\tau^*}{\tau_c} \right)^p \right]^q, \quad (28)$$

where H_0 is the energy parameter of the dislocation-barrier interaction (enthalpy of activation at $\tau^* = 0$); $0 \leq p \leq 1$ and $1 \leq q \leq 2$ are parameters depending on the distribution of obstacles along the dislocation and the shape of the potential barrier created by the obstacle: q depends on the shape of the barrier, and p depends on the properties of the barrier and the statistics of the distribution of barriers.

It is obvious that (27) can only be used at the stage of well-developed plastic deformation of the material at $\frac{d\tau(\varepsilon; T, \dot{\varepsilon})}{d\dot{\varepsilon}} \ll E$, when the rate of plastic deformation significantly exceeds the rate of elastic deformation. From (27) and (28) it follows:

$$\tau(\varepsilon; T, \dot{\varepsilon}) = \tau_i(\varepsilon; T) + \tau_c \left[1 - \left(\frac{T}{T_0} \right)^{1/q} \right]^{1/p}, \quad \tau^*(T) = \tau_c \left[1 - \left(\frac{T}{T_0} \right)^{1/q} \right]^{1/p}, \quad (29)$$

$$\left(\frac{\partial \tau^*}{\partial \ln \dot{\varepsilon}} \right)_T = \frac{\tau_c}{pqA} \left(\frac{T}{T_0} \right)^{1/q} \left[1 - \left(\frac{T}{T_0} \right)^{1/q} \right]^{(1-p)/p}, \quad T_0 = \frac{H_0}{kA}, \quad A = \ln \left(\frac{\dot{\varepsilon}_0}{\dot{\varepsilon}} \right) \quad (30)$$

According to (29) and (30), the stress $\tau^*(T, \dot{\varepsilon})$ decreases monotonically with increasing temperature, and the value $\left(\frac{\partial \tau^*}{\partial \ln \dot{\varepsilon}} \right)_T$ reaches a maximum at $T_m = p^q T_0$ and becomes zero at $T = 0$ K and $T = T_0$.

It was shown [44] that additional features in the temperature dependences of the plasticity characteristics of metals can appear when the temperature dependences $E(T) = E_0 \eta(T)$ of the elastic modulus are taken into account in (29) and (30) (see Section 3.1). In this case, the temperature dependence of the parameters τ_c , τ_i and H_0 will be determined by $\eta(T)$:

$$\tau_c(T) = \tau_{c0} \eta(T), \quad \tau_i(T) = \tau_{i0} \eta(T), \quad H_0(T) = H_{00} \eta(T) \quad (31)$$

4.6. Low-Temperature Plasticity of the Studied Alloy

The strong temperature dependence $\tau_2(T)$ (Figure 3) indicates the thermally activated nature of plastic deformation, while both Peierls barriers and local barriers can be controlling obstacles to the movement of dislocations.

The elementary act of plastic deformation in the first case is the thermally activated nucleation of a paired kink on a dislocation segment L in the Peierls relief (Figure 6a); in the second case, thermally activated overcoming of a local barrier by a dislocation segment $L = l_1 + l_2$ (Figure 6b). As a result of the analysis of low-temperature acoustic resonances in the studied HEA, it was established that in it the Peierls stress $\tau_{p1} \approx 4 \cdot 10^6$ Pa for dislocations in the easy slip system is significantly less than the low-temperature values of the yield strength $\tau_{0.2}, \tau_2 \approx (2 \div 3) \cdot 10^8$ Pa $\approx 50 \cdot \tau_{p1}$. Consequently, the Peierls relief cannot have a significant effect on the kinetics of low-temperature plastic deformation of this material; it can only be controlled by a sufficiently high volume density of local barriers.

The role of structural inhomogeneities that determine thermally activated plastic deformation of HEA can be played by clusters of atoms of one of the constituent elements of the alloy. Several adjacent atoms of an element with a relatively large atomic radius create local distortions of the crystal lattice and are a significant obstacle to dislocations. Such clusters were experimentally observed in [23] and the characteristic distance between them is several nanometers, i.e. for them $L \approx 10$ nm (see section 4.3).

To check the adequacy of the results of an experimental study of the alloy (Figure 3) to the assumption of the controlling influence of these local defects on the kinetics of its plastic deformation at low temperatures, we use the relations obtained from (29) and (30) at values $\varepsilon = 0.02$, $\dot{\varepsilon} = 4 \cdot 10^{-4}$ s⁻¹ and $\tau_i(\varepsilon = 0.02; T) = \tau_{i2}(T)$:

$$\tau_2(T) = \tau_{i2}(T) + \tau_c \left[1 - \left(\frac{T}{T_0} \right)^{\frac{1}{q}} \right]^{\frac{1}{p}}, \quad \gamma(T) = \frac{\tau_c}{pqA} \left(\frac{T}{T_0} \right)^{\frac{1}{q}} \left[1 - \left(\frac{T}{T_0} \right)^{\frac{1}{q}} \right]^{\frac{1-p}{p}}. \quad (32)$$

The parameter A (Figure 3b) were obtained using experimental dependences $\tau_2(T)$, $\gamma(T)$ and relations (30):

$$A = -T \left[\frac{\Delta \tau_2(T)}{\Delta T} \right] \cdot \left[\frac{\Delta \tau_2(T)}{\Delta \ln \dot{\varepsilon}} \right]_T^{-1}. \quad (33)$$

The absence of deviations A from the average value $\bar{A} \approx 19$ with temperature changes justifies the neglect of the weak temperature dependence of the parameter $\dot{\varepsilon}$ in (27) and it is one of the criteria for the applicability of relations (29)-(32) for describing low-temperature thermally activated deformation of metals. Approximations (31)-(32) of experimental data are shown by solid lines in Figure 3, and the parameters τ_{i2} , τ_c , p , q , T_0 are given in Table 4.

Agreement between analytical and experimental points in Figure 4 confirms the adequacy of the theoretical model used and allows us to speak about a single mechanism that controls thermally activated plasticity in the alloy under study in the studied temperature range at $\varepsilon \approx 2\%$. The activation energy in the absence of applied stress $H_0 \approx 0.5\text{--}1$ eV is typical for processes in metals associated with thermally activated movement of dislocations through local barriers [43].

Given in Table 4 model parameters and algorithm [44] for thermal activation analysis of experimental results make it possible to obtain estimates for the parameters of local barriers and the distances between them in slip planes. When dislocations move through a network of randomly located local obstacles, various physical situations can occur, among which two limiting cases stand out. These cases correspond to the Mott-Labusch statistics [48], in which $p = 1$, and the Friedel statistics [38], in which $p = 2/3$. In our case $p \approx 0.6$, which better corresponds to the Friedel statistics, therefore:

$$L(\tau^*) = \left(\frac{2\Gamma S_0}{b\tau^*} \right)^{1/3}, \quad (34)$$

where S_0 is the average area per local obstacle. The stress of activation-free detachment of a dislocation from a barrier is determined by the condition

$$f_m = b \tau_c L(\tau_c). \quad (35)$$

Using (34) and (35), we obtain an expression for the value of S_0 , which allows us to estimate the density of local obstacles that control the movement of the dislocation

$$S_0 = \frac{f_m^3}{2b^2 \Gamma \tau_c^2}. \quad (36)$$

The value of $q \approx 1$ indicates that the force barrier has steep slopes and its shape is close to rectangular in the range of values τ^* that were achieved in our experiments. Therefore, the width w of the force barrier will weakly depend on τ^* , and for the value of the maximum force the following estimate will be true: $f_m = H_0 / w$. Using this estimate and expression (36), we obtain:

$$S_0 = \frac{H_0^3}{2b^2 w^3 \Gamma \tau_c^2} = \frac{H_0^3}{2b^5 \Gamma \tau_c^2} \left(\frac{b}{w} \right)^3. \quad (37)$$

Using (37), and the values H_0 and τ_c from the Table 1, we get the estimate $S_0 = 1.7 \cdot 10^{-17} (b/w)^3$, m^2 . Taking $w \sim b$, we obtain an upper estimate for the value $S_0 = 261 b^2$, which corresponds to the distance between local obstacles in the sliding plane $l = (S_0)^{1/2} = 16 b = 4.1 \text{ nm}$ and $L = 2l \approx 10 \text{ nm}$.

Table 4. Parameters of the dislocation theory of plasticity for HEA $\text{Al}_{0.5}\text{CoCrCuFeNi}$ in state (I).

| p | q | τ_{i2} , MPa | τ_c , MPa | H_0 , eV | T_0 , K | A |
|-----|-----|-------------------|----------------|------------|-----------|-----|
| 0.6 | 1.1 | 170 | 104 | 0.65 | 400 | 19 |

5. Conclusion

Analysis and physical interpretation based on modern dislocation theory of the results of a comprehensive experimental study [21,22] of the processes of plastic deformation and acoustic relaxation in HEA $\text{Al}_{0.5}\text{CoCrCuFeNi}$ made it possible to establish:

- the most important types of dislocation defects in the lattice structure of the alloy;
- types of barriers that prevent the movement of dislocation lines (strings);
- adequate mechanisms of thermally activated movement of various elements of dislocation strings through barriers under conditions of moderate and deep cooling;
- quantitative estimates for the most important characteristics of dislocations and their interaction with barriers.

References

- Yeh, J.; Chen, S.; Lin, S.; Gan, J.; Chin, T.; Shun, T.; Tsau, C.; Chang, S. Nanostructured High-Entropy Alloys with Multiple Principal Elements: Novel Alloy Design Concepts and Outcomes *Adv. Eng. Mater.* **2004**, *6*, 299-303. <https://doi.org/10.1002/adem.200300567>
- Cantor, B.; Chang I.T.H.; Knight P.; Vincent A.J.B. Microstructural development in equi-atomic multicomponent alloys *Mater. Sci. Eng. A* **2004**, *375-377*, 213-218. <https://doi.org/10.1016/j.msea.2003.10.257>
- Cantor, B. Multicomponent high-entropy Cantor alloys. *Prog. Mater. Sci.* **2021**, *120*, 100754. <https://doi.org/10.1016/j.pmatsci.2020.100754>
- Kao, Y.F.; Chen, T.J.; Chen, S.K.; Yeh, J.W. Microstructure and mechanical property of as-cast, homogenized and deformed $\text{Al}_x\text{CoCrFeNi}$ ($0 \leq x \leq 2$) high-entropy alloys. *J. Alloys Compd.* **2009**, *488*, 57-64. <https://doi.org/10.1016/j.jallcom.2009.08.090>
- Tabachnikova, E.D.; Podolskiy, A.V.; Laktionova, M.O.; Bereznaya, N.A.; Tikhonovsky, M.A.; Tortika, A.S. Mechanical properties of the CoCrFeNiMnVx high entropy alloys in temperature range 4.2-300 K. *J. Alloys Compd.* **2017**, *698*, 501-509. <https://doi.org/10.1016/j.jallcom.2016.12.154>

6. Gludovatz, B.; Ritchie, R.O. Fracture properties of high-entropy alloys. *MRS Bulletin* **2022**, *47*, 176–185. <https://doi.org/10.1557/s43577-022-00267-9>
7. Chen, S.; Oh, H.S.; Gludovatz, B.; Kim, S.J.; Park, E.S.; Zhang, Z.; Ritchie, R.O.; Yu, Q. Real-time observations of TRIP-induced ultrahigh strain hardening in a dual-phase CrMnFeCoNi high-entropy alloy. *Nat. Commun.* **2020**, *11*, 826. <https://doi.org/10.1038/s41467-020-14641-1>
8. Pogrebnyak, A.D.; Yakushchenko, I.V.; Bagdasaryan, A.A.; Bondar, O.V.; Krause-Rehberg, R.; Abadias, G.; Chartier, P.; Oyoshi, K.; Takeda, Y.; Beresnev, V.M.; Sobol, O.V. Microstructure, physical and chemical properties of nanostructured (Ti–Hf–Zr–V–Nb) N coatings under different deposition conditions. *Mater. Chem. Phys.* **2014**, *147*, 1079–1091. <https://doi.org/10.1016/j.matchemphys.2014.06.062>
9. Laktionova, M.A.; Tabachnikova, E.D.; Tang, Z.; Liaw, P.K. Mechanical properties of the high-entropy alloy Al_{0.5}CoCrCuFeNi at temperatures of 4.2–300 K. *Low Temp. Phys.* **2013**, *39*, 630–632. <https://doi.org/10.1063/1.4813688>
10. Moon, J.; Tabachnikova, E.; Shumilin, S.; Hryhorova, T.; Estrin, Y.; Brechtl, J.; Liaw, P.; Wang, W.; Dahmen, K.A.; Kim, H.S. Unraveling the discontinuous plastic flow of a Co–Cr–Fe–Ni–Mo multiprincipal-element alloy at deep cryogenic temperatures. *Phys. Rev. Materials.* **2021**, *5*, 083601. <https://doi.org/10.1103/PhysRevMaterials.5.083601>
11. Heczel, A.; Kawasaki, M.; Lábár, J.L.; Jang, J.-il; Langdon, T.G.; Gubicza. Defect structure and hardness in nanocrystalline CoCrFeMnNi high-entropy alloy processed by high-pressure torsion. *Alloys Compd.* **2017**, *711*, 143–154. <https://doi.org/10.1016/j.jallcom.2017.03.352>
12. Naeem, M.; He, H.; Zhang, F.; Huang, H.; Harjo, S.; Kawasaki, T.; Wang, B.; Lan, S.; Wu, Z.; Wang, F.; Wu, Y.; Lu, Z.; Zhang, Z.; Liu, C.T.; Wang, X.-L. Cooperative deformation in high-entropy alloys at ultralow temperatures *Sci. Adv.* **2020**, *6*, eaax4002. <https://doi.org/10.1126/sciadv.aax4002>
13. Tabachnikova, E.; Hryhorova, T.; Shumilin, S.; Semerenko, Y.; Huang, Y.; Langdon, T. Cryo-severe plastic deformation, microstructures and properties of metallic nanomaterials at low temperatures. *Mater. Trans.* **2023**, *64*, 1806–1819. <https://doi.org/10.2320/matertrans.MT-MF2022037>
14. Liu, X.; Ding, H.; Huang, Y.; Bai, X.; Zhang, Q.; Zhang, H.; Langdon, T.G.; Cui, J. Evidence for a phase transition in an AlCrFe₂Ni₂ high entropy alloy processed by high-pressure torsion. *J. Alloys Compd.* **2021**, *867*, 159063. <https://doi.org/10.1016/j.jallcom.2021.159063>
15. Levenets, A.V.; Rusakova, H.V.; Fomenko, L.S.; Huang, Y.; Kolodiy, I.V.; Vasilenko, R.L.; Tabachnikova, E.D.; Tikhonovsky, M.A.; Langdon, T.G. Structure and low-temperature micromechanical properties of as-cast and SPD-processed high-entropy Co_{25-x}Cr₂₅Fe₂₅Ni₂₅C_x alloys. *Low Temp. Phys.* **2022**, *48*, 560–569. <https://doi.org/10.1063/10.0011605>
16. Lee, D.H.; Choi, I.C.; Seok, M.Y.; He, J.; Lu, Z.; Suh, J.-Y.; Kawasaki, M.; Langdon, T.G.; Jang, J.-il. Nanomechanical behavior and structural stability of a nanocrystalline CoCrFeNiMn high-entropy alloy processed by high-pressure torsion *J. Mater. Res.* **2015**, *30*, 2804–2815. <https://doi.org/10.1557/jmr.2015.239>
17. Moon, J.; Qi, Y.; Tabachnikova, E.; Estrin, Yu.; Choi, W.-Mi.; Joo, S.-H.; Lee, B.-J.; Podolskiy, A.; Tikhonovsky, M.; Kim, H.S. Microstructure and Mechanical Properties of High-Entropy Alloy Co₂₀Cr₂₆Fe₂₀Mn₂₀Ni₁₄ Processed by High-Pressure Torsion at 77 K and 300 K. *Sci. Rep.* **2018**, *8*, 11074. <https://doi.org/10.1038/s41598-018-29446-y>
18. Tirunilai, A.S.; Hanemann, T.; Reinhart, C.; Tschan, V.; Weiss, K.-P.; Laplanche, G.; Freudenberger, J. Comparison of cryogenic deformation of the concentrated solid solutions CoCrFeMnNi, CoCrNi and CoNi. *Mater. Sci. Eng. A* **2020**, *783*, 139290. <https://doi.org/10.1016/j.msea.2020.139290>
19. Rusakova, A.V.; Fomenko, L.S.; Smirnov, S.N.; Podolskiy, A.V.; Shapovalov, Y.O.; Tabachnikova, E.D.; Tikhonovsky, M.A.; Levenets, A.V.; Zehetbauer, M.J.; Schafler, E. Low temperature micromechanical properties of nanocrystalline CoCrFeNiMn high entropy alloy. *Mater. Sci. Eng. A* **2021**, *828*, 142116. <https://doi.org/10.1016/j.msea.2021.142116>
20. Podolskiy, A.V.; Schafler, E.; Tabachnikova, E.D.; Tikhonovsky, M.A.; Zehetbauer, M.J. Thermally activated deformation of nanocrystalline and coarse grained CoCrFeNiMn high entropy alloy in the temperature range 4.2–350 K *Low Temp. Phys.* **2018**, *44*, 976–982. <https://doi.org/10.1063/1.5052688>
21. Tabachnikova, E.D.; Laktionova, M.A.; Semerenko, Yu.A.; Shumilin, S.E.; Podolskiy, A.V.; Tikhonovsky, M.A.; Miskuf, J.; Csach, K. Mechanical properties of the high-entropy alloy Al_{0.5}CoCrCuFeNi in various structural states at temperatures of 0.5–300 K. *Low Temp. Phys.* **2017**, *43*, 1108–1118. <https://doi.org/10.1063/1.5004457>

22. Semerenko, Yu.A.; Natsik, V.D. Low temperature peak of internal friction in high entropy $\text{Al}_{0.5}\text{CoCrCuFeNi}$ alloy. *Low Temp. Phys.* **2020**, *46*, 78-86. <https://doi.org/10.1063/10.0000367>

23. Pickering, E.J.; Stone, H.J.; Jones, N.G. Fine-scale precipitation in the high-entropy alloy $\text{Al}_{0.5}\text{CrFeCoNiCu}$. *Mat. Sci. Eng. A* **2015**, *645*, 65-71. <https://doi.org/10.1016/j.msea.2015.08.010>

24. Natsik, V.D.; Semerenko, Yu.A. Dislocation mechanisms of low-temperature acoustic relaxation in iron. *Low Temp. Phys.* **2019**, *45*, 551-567. <https://doi.org/10.1063/1.5097366>

25. Varshni, Y.P. Temperature Dependence of the Elastic Constants. *Phys. Rev. B2* **1970**, *1*, 3952. <https://doi.org/10.1103/PhysRevB.2.3952>

26. Girifalco, L.A. Statistical Physics of Materials; Wiley: New York, NY, 1973; p. 362.

27. Schoeck, G.; Bisogni, E.; Shyne, J. The activation energy of high temperature internal friction. *Acta Metall.* **1964**, *12*, 1466-1468. [https://doi.org/10.1016/0001-6160\(64\)90141-5](https://doi.org/10.1016/0001-6160(64)90141-5)

28. Natsik, V.D.; Semerenko, Yu.A. Dislocation mechanisms of low-temperature internal friction in nanostructured materials. *Low Temp. Phys.* **2016**, *42*, 138-148 <https://doi.org/10.1063/1.4942907>

29. Asgari, S.; El-Danaf, E.; Kalidindi, S.R.; Doherty, R.D. Strain hardening regimes and microstructural evolution during large strain compression of low stacking fault energy fcc alloys that form deformation twins. *Metall. Mater. Trans. A* **1997**, *28*, 1781-1795. <https://doi.org/10.1007/s11661-997-0109-3>

30. Evans, A.; Rawlings, R. The thermally activated deformation of crystalline materials. *Physica Status Solidi*, **1969**, *34*, 9-31. <https://doi.org/10.1002/pssb.19690340102>

31. Niblett, D.H. Bordoni Peak in Face-Centered Cubic Metals. In Ed.: Mason, W.P. Physical Acoustics: Principles and Methods. Volume III, Part A. The Effect of Imperfections; Academic Press: New York, NY, 1966; p. 428

32. Chambers, R. Dislocation relaxations in Base-Centered Cubic Transition Metals. In Ed.: Mason, W.P. Physical Acoustics, Volume III, Part A; Academic Press: New York, NY, 1964; p. 428

33. Bordoni, P.G. Elastic and anelastic behavior of some metals at very low temperatures. *Journ. Acoust. Soc. Amer.* **1954**, *26*, 495-502. <https://doi.org/10.1121/1.1907363>

34. Postnikov, V.S. Internal Friction in Metals and Alloys, 1st ed.; Springer: New York, NY, 1967., p. 266

35. Seeger, A. On the theory of the low-temperature internal friction peak observed in metals. *Phil. Mag.* **1956**, *1*, 651-662 <https://doi.org/10.1080/14786435608244000>

36. Seeger, A.; Schiller, P. Kinks in Dislocation Lines and their Effects on the Internal Friction in Crystals. In Ed.: Mason, W.P. Physical Acoustics, Volume III, Part A; Academic Press: New York, NY, 1964; p. 428

37. Seeger, A.; Wüthrich, C. Dislocation relaxation processes in body-centred cubic metals. *Nuovo Cimento B*, **1976**, *33*, 38-75. <https://doi.org/10.1007/BF02722472>

38. Friedel, J. Dislocations; Pergamon Press: Oxford, 1964; p. 491

39. Anderson, P.M.; Hirth, J.P.; Lothe, J. Theory of Dislocations, 3rd ed.; Cambridge University Press: Cambridge, 2017; p. 699

40. Koiwa, M.; Hasiguti, R.R. A theory of internal friction peak due to thermal unpinning of dislocations and its application to P1 peak in copper. *Acta Met.* **1965**, *13*, 1219-1230. [https://doi.org/10.1016/0001-6160\(65\)90032-5](https://doi.org/10.1016/0001-6160(65)90032-5)

41. Fitzgerald, S.P. Kink pair production and dislocation motion. *Sci. Rep.* **2016**, *6*, 39708. <https://doi.org/10.1038/srep39708>

42. Utt, D.; Lee, S.; Xing, Y.; Jeong, H.; Stukowski, A.; Oh, S.H.; Dehm, G.; Albe, K. The origin of jerky dislocation motion in high-entropy alloys. *Nat. Commun.* **2022**, *13*, 4777. <https://doi.org/10.1038/s41467-022-32134-1>

43. Pustovalov, V.V.; Fomenko, V.S. Plastic deformation of crystals at low temperatures. Naukova Dumka; Kiev 2012; p. 356.

44. Moskalenko, V.A.; Natsik, V.D.; Kovaleva, V.N. The role of Peierls relief in the low-temperature plasticity of pure α -Ti. *Low Temp. Phys.* **2005**, *31*, 907-914. <https://doi.org/10.1063/1.2126949>

45. Kocks, U.F.; Argon, A.S.; Ashby, M.F. Thermodynamics and Kinetics of Slip, 1st ed.; Progress in Materials Science; Pergamon Press: Oxford, **1975**; p.288

46. Schwarz, B.; Isaac, R.D.; Granato, A.V. Dislocation Inertial Effects in the Plastic Deformation of Dilute Alloys of Lead and Copper. *Phys. Rev. Lett.* **1977**, *38*, 554-557. <https://doi.org/10.1103/PhysRevLett.38.554>

47. Isaev, N.V.; Natsik, V.D.; Pustovalov, V.V.; Fomenko, V.S.; Shumilin, S.E. Low-temperature plasticity of Pb-Bi alloys: the role of thermal activation and inertial effects. *Low Temp. Phys.* **1998**, *24*, 593-601. <https://doi.org/10.1063/1.593640>

48. Schwarz, B.; Labusch, R.J. Dynamic simulation of solution hardening. *J. Appl. Phys.* **1978**, *49*, 5174-5187. <https://doi.org/10.1063/1.324413>
49. Bulatov, O.S.; Klochko, V.S.; Korniyets, A.V.; Kolodiy, I.V.; Kondratov, O.O.; Tikhonovska, T.M. Low temperature elastic properties of $Al_{0.5}CoCrCuFeNi$ high-entropy alloy. *Funct. Mater.* **2021**, *28*, 492-496. <https://doi.org/10.15407/fm28.03.492>

Disclaimer/Publisher's Note: The statements, opinions and data contained in all publications are solely those of the individual author(s) and contributor(s) and not of MDPI and/or the editor(s). MDPI and/or the editor(s) disclaim responsibility for any injury to people or property resulting from any ideas, methods, instructions or products referred to in the content.